Asymmetry in the percolation thresholds of fully penetrable disks with two different radii

John A. Quintanilla*
Department of Mathematics, P.O. Box 311430, University of North Texas, Denton, Texas 76203, USA

Robert M. Ziff†
Department of Chemical Engineering, University of Michigan, Ann Arbor, Michigan 48109-2136, USA

(Received 29 June 2007; published 14 November 2007)

We perform simulations of continuum gradient percolation to measure the percolation threshold of systems of fully penetrable disks of two different radii. As a function of volumetric proportion v, the percolation threshold $\phi_c(v,\lambda)$ is approximately symmetric about $v=0.5$ for a fixed ratio λ of the radii. However, the difference from symmetry is strongly statistically significant. We also improve, by an order of magnitude, the measurement of the percolation threshold for disks of equal radius: $\phi_c^*=0.676\,347\,5(6)$.

DOI: 10.1103/PhysRevE.76.051115 PACS number(s): 64.60.Ak, 05.20.−y, 61.43.Hv

I. INTRODUCTION

Measurements of the continuum percolation threshold of various models have received much attention in the literature. One of these models is a Boolean model with grains of some specified shape positioned upon the points of an underlying Poisson process [1,2]. For example, in two dimensions, models that have been recently studied include equal-sized fully penetrable disks [3,4], disks with two different radii [5–8], aligned and randomly oriented squares [9], aligned squares of two different side lengths [10], and randomly oriented ellipses [11,12]. In three dimensions, recent studies include the percolation thresholds of equal-sized fully penetrable spheres [13], spheres with two different radii [14], aligned and randomly oriented cubes [9], aligned cubes of two different side lengths [10], and randomly oriented ellipsoids [12]. Furthermore, in three dimensions, the *void* percolation threshold has been measured for equal-sized spheres and spheres of two different radii [15–17] as well as for randomly oriented ellipsoids [18].

Continuum percolation also continues to be studied from the perspective of stochastic geometry as well as statistical physics, and multiple mathematical techniques have been developed to rigorously analyze percolation thresholds [19–25]. Tight rigorous bounds have been published on the percolation threshold for disks and aligned squares [25]; in the latter case, the tightness of these bounds actually exceeds the best current measurement of the threshold from computer simulations.

In this paper, we reconsider measurement of the percolation threshold of binary dispersions of disks with two different radii R and λR, where $0\leqslant\lambda\leqslant 1$. Also, the proportion of the smaller and larger disks is p and $1-p$, respectively, so that $0\leqslant p\leqslant 1$, and the disks are positioned independently of each other and the underlying Poisson field. The parameters p and λ determine the critical volume fraction for the binary dispersion.

Recently [26], it was suggested that the percolation threshold may be written in terms of λ and the *volumetric* proportion of smaller disks v, which is given by

$$v=\frac{p\pi(\lambda R)^2}{p\pi(\lambda R)^2+(1-p)\pi R^2}=\frac{p\lambda^2}{p\lambda^2+1-p}. \tag{1}$$

It was conjectured that the percolation threshold is a symmetric function of v, so that

$$\phi_c(v,\lambda)=\phi_c(1-v,\lambda). \tag{2}$$

This was based upon available numerical results, and a theoretical argument for this symmetry was also presented.

In this paper, we first use efficient numerical techniques to find this threshold to much higher precision. We show with a high degree of confidence that the graphs of $\phi_c(v,\lambda)$ are not symmetric in v, so that Eq. (2) cannot be exactly true. We also show that the theoretical arguments given in [26] are not sufficient to show that ϕ is symmetric in v.

Second, with our numerical results, we study the value of $v^*(\lambda)$, defined to be the value of v which maximizes $\phi(v,\lambda)$ for a prescribed λ. Specifically, we investigate the conjecture that

$$v^*(\lambda)=1/2 \quad \text{for all } \lambda, \tag{3}$$

or, equivalently, that $p^*(\lambda)=1/(1+\lambda^2)$. This behavior is consistent with an earlier conjecture that, for small λ, $p^*(\lambda)=1-\lambda^2$ [7]. Although asymmetry does not preclude Eq. (2), it does suggest that Eq. (3) is false. In any case, we find that $v^*(\lambda)$ is indeed near $1/2$, but we cannot conclusively disprove Eq. (3) because of the inherent numerical errors in measuring $v^*(\lambda)$. However, this negative result does not contradict our conclusion that the curves, overall, are asymmetric.

In Sec. II, we summarize the techniques used to produce our improved numerical estimates for $\phi_c(v,\lambda)$. In Sec. III, we discuss the asymmetry of $\phi_c(v,\lambda)$ in light of these improved estimates, and examine the theoretical argument given in [26] that these curves should be exactly symmetric.

*jquintanilla@unt.edu; URL: http://www.math.unt.edu/~johnq
†rziff@umich.edu

 ©2007 The American Physical Society

II. BINARY DISPERSIONS

A. Frontier-walk method

A variety of techniques were used in the two- and three-dimensional studies mentioned in the Introduction. In this paper, we primarily use the technique of continuum gradient percolation, simulating disks that are centered on the points of an underlying inhomogeneous Poisson field [1]. Selected measurements were confirmed by using the cluster growth technique [9,12,13,27].

To begin, an inhomogeneous Poisson field is dynamically simulated in a unit square. That is, instead of simulating the entire Poisson field inside of the square all at once, only the portions of the square that are nearest to the current location of the walk are simulated. Dynamic simulation provides significant savings with regard to both time and computational resources. As the points of the inhomogeneous Poisson field are dynamically generated, they are assigned to be the centers of disks of radius R or λR with probabilities $1-p$ and p, respectively. For each point, this assignment is made independently of both the assignments for all other points and the Poisson field itself.

The percolation threshold is measured using the continuum frontier-walk method [4,28,29,34], which we now describe. To start the simulation, the right half of the top of the square is initialized with overlapping disks with centers a radius apart. The walk is started at the leftmost point of these initial disks and initially traverses the lower portion of the disks. After a while, the walk continues inside the square. By carefully reinitializing the Poisson field as the walk progresses, a walk of infinite length may be generated on a computer with finite memory [4].

The percolation threshold is estimated by measuring the average location of the frontier, or the average location of the arcs on the edge of the percolating cluster which naturally forms [3,4,28]. We denote these estimated values by $\phi_c(v,\lambda,L)$, where the length scale L is defined to be the ratio between the side of the square and the radius R of the larger disks. In this study, we used five choices of length scales: $L=12\,500\times 2^n$ for $0\leqslant n\leqslant 4$.

B. Error analysis

Each estimate $\phi_c(v,\lambda,L)$ has a standard error $\sigma(\lambda)$, which depends on the number of configurations attempted. In this study, we chose a desired value of $\sigma(\lambda)$ as a stopping condition for the algorithm. Also, we chose σ to be a function of only λ and not of v or L. Due to computational cost, we chose to perform somewhat less refined measurements of $\phi_c(v,\lambda)$ for $\lambda\leqslant 0.7$ than for $0.76\leqslant\lambda\leqslant 0.96$.

This data are then fitted to the model

$$\phi_c(v,\lambda,L)=\frac{m(v,\lambda)}{L}+\phi_c(v,\lambda), \tag{4}$$

where $m(v,\lambda)$ and $\phi_c(v,\lambda)$ are computed from the data. This computation of $\phi_c(v,\lambda)$ has the effect of extrapolating to the limit $L\to\infty$.

Figure 1 illustrates this fitting for four different choices of (v,λ); the y intercepts of the regression lines correspond to the estimates presented here. The error bars in Fig. 1 represent one standard deviation. The wider error bars for $\lambda\leqslant 0.70$ are reflected in Fig. 1 for the case of $\lambda=0.35$. We observed that the residuals of the data were consistent with the standard error $\sigma(\lambda)$, thus providing an important verification of the appropriateness of the model (4). We also found that the correlation coefficient of the five points tended to decrease as λ decreased.

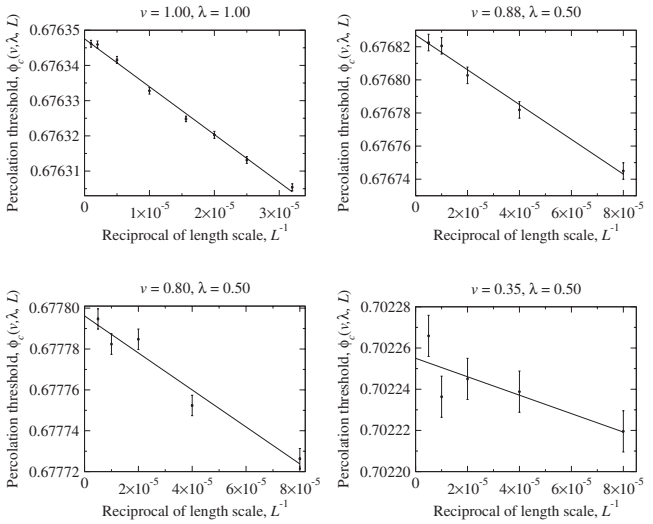

FIG. 1. Estimates of the percolation threshold $\phi_c(v,\lambda,L)$ for four different choices of (v,λ). For $\lambda<1$, the five length scales $L=12\,500\times 10^n$ for $n=0,\ldots,4$ are simulated. Due to computational cost, the error bars for $\lambda\leqslant 0.7$ are twice as wide as for $0.76\leqslant\lambda\leqslant 0.96$. For the special case of equal-sized disks, very narrow error bars are prescribed, and the values of L used are 31 250, 40 000, 50 000, 64 000, 10^5, 2×10^5, 5×10^5, and 10^6. The y intercepts of the regression lines correspond to the estimates of $\phi_c(v,\lambda)$ reported in this paper, which may be found in [33] as well as Eq. (6) for the case of equal-sized disks.

Since, for each λ, $\sigma(\lambda)$ is chosen the same for all length scales, the standard error for the estimate $\phi_c(v,\lambda)$ is given by [32]

$$\text{standard error}=\sigma(\lambda)\sqrt{\frac{\sum_{i=1}^{n}(1/L_i^2)}{n\sum_{i=1}^{n}(1/L_i^2)-\left(\sum_{i=1}^{n}(1/L_i)\right)^2}}, \tag{5}$$

where $L_1,\ldots,L_n$ are the lengths scales that are used. Using this formula, the standard error (that is, one standard deviation) is 6.8×10^{-6} for all estimates reported for $\lambda\leqslant 0.76$, while the analogous error is 3.4×10^{-6} for $\lambda\geqslant 0.8$ [33].

To produce these results to this level of accuracy, a bank of 2.6-GHz microcomputers were used for a collective 13.6 yr of runtime to generate and measure an aggregate of 16.0 trillion frontier arcs. Larger values of L and smaller values of λ required greater computational effort. To give one example, the five length scales used for the case (v,λ)

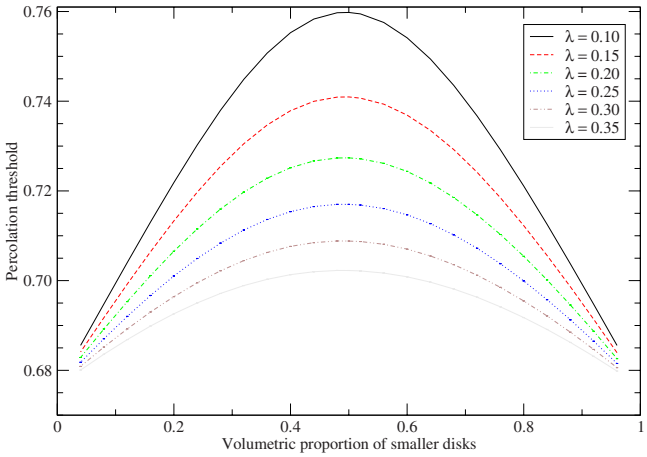

FIG. 2. (Color online) Estimates of the percolation threshold $\phi_c(v,\lambda)$ for $0.10 \leqslant \lambda \leqslant 0.35$. The error bars for each point are comparable to the thickness of the lines on the scale of this figure.

$=(0.2,0.5)$ each used from 1.7 to 2.4 billion frontier arcs, totaling more than 10 billion frontier arcs.

III. MEASUREMENTS OF THE PERCOLATION THRESHOLD

A. Results

These improved estimates for $\phi_c(v,\lambda)$ are given in [33] and are plotted in Figs. 2–4. Where comparable, these estimates are within the error bars of the most precise previous estimates [7]. Our improved estimates are also clearly consistent with the conjecture that the percolation threshold is minimized in the monodisperse limit of $\lambda=1$ [7,14,21].

We also reconsidered measurement of the critical volume fraction ϕ_c^* for disks of equal size. We repeated, with the more powerful computational resources now available to us, the measurement of ϕ_c^* using continuum gradient percolation as described in [4]. To improve accuracy for this important

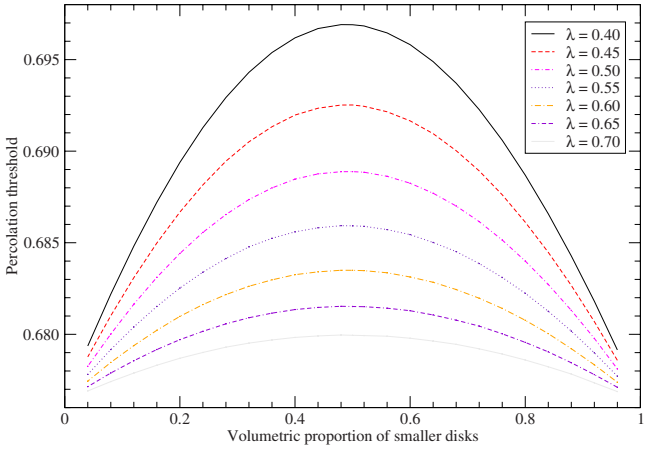

FIG. 3. (Color online) Estimates of the percolation threshold $\phi_c(v,\lambda)$ for $0.40 \leqslant \lambda \leqslant 0.70$. The error bars for each point are comparable to the thickness of the lines on the scale of this figure.

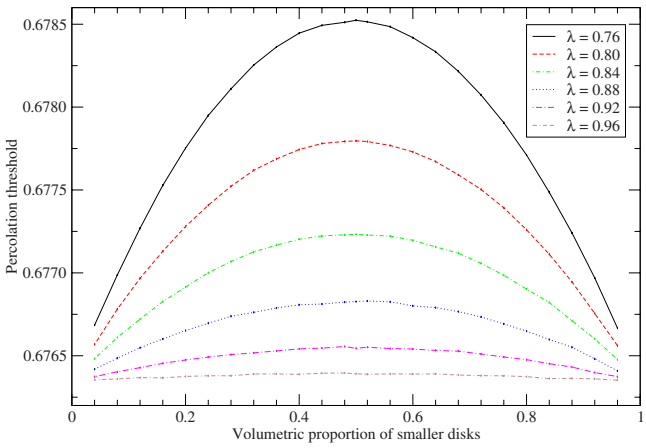

FIG. 4. (Color online) Estimates of the percolation threshold $\phi_c(v,\lambda)$ for $0.76 \leqslant \lambda \leqslant 0.96$. The error bars for each point are comparable to the thickness of the lines on the scale of this figure.

special case, estimates with somewhat narrower error bars than for the true binary dispersions considered above are computed. Also, we used all of the above values of L as well as $L=31\,250$, $40\,000$, $64\,000$, 5×10^5, and 10^6.

With the narrower error bars used for equal-sized disks, we observed that the residuals of the model (4) did not follow the assumptions of the standard linear regression model. First, the maximum residual was roughly 3.4 standard deviations. Second, there was an observable curve in the data points, so that the residuals were heteroscedastic. These observations are not surprising since the empirical model (4) is expected to be valid only for large values of L. Accordingly, we chose not to use the values of $L=12\,500$ and $L=25\,000$ to estimate the percolation threshold for equal-sized disks. By omitting these smallest values of L, the residuals appeared to follow the assumptions of the standard linear regression model. (We note that none of these difficulties were observed for true binary dispersions, which were measured with wider error bars in this study.)

All of these refinements are reflected in Fig. 1. With this work, our updated measurement of the percolation threshold for equal-sized disks is

$$\phi_c^* = 0.676\,347\,5(6), \tag{6}$$

where the parentheses indicate an error of one standard deviation in the last decimal place. This result adds an extra decimal place of accuracy to the most precise previous estimate [4],

$$\phi_c^* = 0.676\,339(6). \tag{7}$$

We made several attempts to fit the data in [33] to a single function; the best function that we found is

$$\phi_c(v,\lambda) = 1 - e^{-\eta(v,\lambda)}, \tag{8}$$

where

$$\eta(v,\lambda) = \eta_c^* a(\lambda) v^{b(\lambda)} (1-v)^{c(\lambda)} \tag{9}$$

with $\eta_c^* = -\ln(1-\phi_c^*)$ and the values of $a(\lambda)$, $b(\lambda)$, and $c(\lambda)$ are presented in [33]. Equation (9) is proportional to the

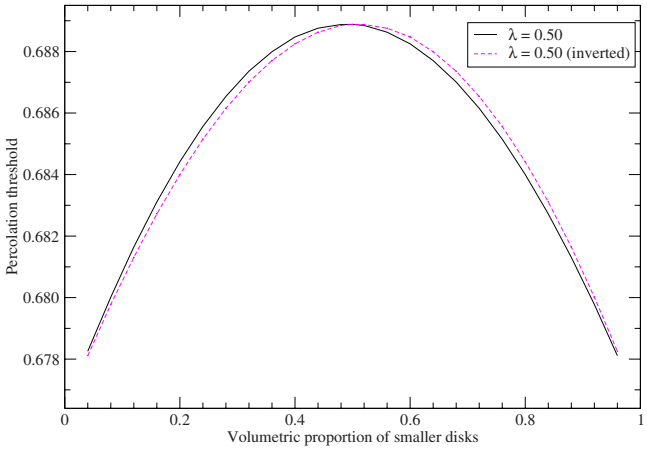

FIG. 5. (Color online) Estimates of the percolation threshold $\phi_c(v,0.5)$. The dashed line is the graph of $\phi_c(1-v,0.5)$, showing that $\phi_c(v,0.5)$ is slightly asymmetric about the line $v=0.5$. The error bars for each point are comparable to the thickness of the lines on the scale of this figure.

probability density function (pdf) of a beta distribution with parameters $b(\lambda)$ and $c(\lambda)$ [30].

The form (8) is motivated by the well-known expression for the volume fraction of a Boolean model [1,31]. The terms v and $1-v$ terms in Eq. (9) are motivated by the following boundary conditions on $\phi_c(v,\lambda)$:

$$\phi_c(0,\lambda) = \phi_c(1,\lambda) = \phi_c(v,0) = \phi_c(v,1) \equiv \phi_c^*; \qquad (10)$$

the degenerate case $v=1$, $\lambda=0$ is obviously not considered in the above boundary conditions.

B. Analysis of symmetry

We notice that the graphs in Figs. 2–4 are approximately symmetric. However, most of these curves are slightly but demonstrably asymmetric. To give one example, Fig. 5 reproduces the graph of $\phi_c(v,0.5)$ from Fig. 3; the dashed line shows the graphs of $\phi_c(1-v,0.5)$. If $\phi_c(v,0.5)$ were perfectly symmetric, then the two graphs should be identical. However, the figure clearly shows that $\phi_c(v,0.5)$ is slightly asymmetrical about the line $v=0.5$.

For a more quantitative analysis, we define $X(v,\lambda)$ to be a random variable representing measurements of $\phi_c(v,\lambda)$. Since each measurement reported in [33] is formed by averaging many simulations, we may reasonably assume each $X(v,\lambda)$ has a normal distribution with mean $\phi_c(v,\lambda)$ and standard deviation $\sigma(\lambda)$.

To test the symmetry of $\phi_c(v,\lambda)$, we consider the test statistic

$$T_1(\lambda) = \sum_{n=1}^{12} \frac{[X(0.04n,\lambda) - X(1-0.04n,\lambda)]^2}{2\sigma(\lambda)^2}. \qquad (11)$$

Our null hypothesis is that, for all n, $X(0.04n,\lambda)$ and $X(1-0.04n,\lambda)$ have the same mean. Under this null hypothesis, $T_1(\lambda)$ has a χ^2 distribution with 12 degrees of freedom, and so we may use its complementary cumulative distribution function (cdf) to test the symmetry of $\phi_c(v,\lambda)$.

The test statistics $T_1(\lambda)$ and the observed significance levels are presented in [33]. For all $\lambda \leqslant 0.84$, the asymmetry of $\phi_c(v,\lambda)$ is strongly statistically significant. In fact, even if the standard errors were $\sigma(\lambda)$ were arbitrarily increased by a factor of 10, the asymmetry would remain statistically significant for $\lambda \leqslant 0.6$. We therefore conclude the $\phi_c(v,\lambda)$ is not perfectly symmetric about $v=0.5$.

With this numerical evidence in mind, we now turn to the heuristic argument presented in [26]. The authors of that work write v of Eq. (1) in terms of the numbers of small and large disks, N_a and N_b, respectively:

$$v = \frac{N_a v_a}{N_a v_a + N_b v_b}, \qquad (12)$$

where $v_a = \pi(\lambda R)^2$ and $v_b = \pi R^2$ are the volumes of the two disk types, and $N_a/(N_a+N_b)=p$. In terms of these quantities, the volume fraction occupied by the disks in the binary system is given by $\phi = 1-e^{-\eta}$, where

$$\eta = \frac{N_a v_a + N_b v_b}{V} \qquad (13)$$

and V is the total volume.

Now, Consiglio *et al.* made the observation that if one replaces N_a and N_b by

$$N_a' = \frac{v_b}{v_a} N_b = N_b/\lambda^2,$$

$$N_b' = \frac{v_a}{v_b} N_a = N_a\lambda^2, \qquad (14)$$

then the value of η' given by Eq. (13) remains unchanged. Thus, they argued, if the original system were at the percolation threshold, then the transformed system would also be at the threshold, presumably because the volume fraction ϕ is unchanged. The transformed particle numbers in Eq. (14) imply $v'=1-v$, and so this argument would seem to prove Eq. (3).

The apparent flaws of this argument are as follows: (i) Just because the volume fraction is unchanged when making the above transformation, it does not follow that the transformed system will also be at the critical threshold—being at the threshold involves more than having a certain volume fraction. (ii) Furthermore, it should be noted that in the transformation (14), besides making $v'=1-v$, it also follows that the total number of particles $N=N_A+N_B$ transforms in a very specific way:

$$N' = N\left(\frac{1-p}{\lambda^2} + \lambda^2 p\right). \qquad (15)$$

In other words, just making $v'=1-v$ is not sufficient to make $\phi'=1-\phi$; N must also transform as above. There is no obvious reason why this transformation in N should be made, and if it were made, whether it should keep the system at a critical point. Equation (15) in fact, follows from the requirement that ϕ remain unchanged when $v'=1-v$. Thus there

appears to be no theoretical reason that Eq. (2) should be true.

We also note that the symmetry of a curve may be measured with the skewness, or the ratio of the centralized third moment to the cube of the standard deviation. For the empirical fit given by Eq. (9), the skewness is given by

$$\text{skewness} = \frac{2[c(\lambda) - b(\lambda)]}{2 + b(\lambda) + c(\lambda)} \sqrt{\frac{1 + b(\lambda) + c(\lambda)}{b(\lambda)c(\lambda)}}. \quad (16)$$

The computed skewness values for the empirical fit (9) is shown in [33].

C. Analysis of maximum values

We observe in [33] that the maximum value of $\phi_c(v,\lambda)$ typically occurs near $v=0.5$. However, in several cases, the largest measured value of $\phi_c(v,\lambda)$ does not occur exactly at $v=0.5$.

To test whether $\phi_c(v,\lambda)$ is maximized at $v=0.5$ for each λ, we consider the test statistic

$$T_2(h,\lambda) = \frac{X(0.5,\lambda) - M}{\sigma(\lambda)}, \quad (17)$$

where

$$M = \max\{X(0.5+h,\lambda), X(0.5-h,\lambda)\} \quad (18)$$

and $X(v,\lambda)$ and $\sigma(\lambda)$ are as before. Our null hypothesis is that $\phi_c(0.5,\lambda) = \phi_c(0.5 \pm h,\lambda)$. Large values of $T_2(h,\lambda)$ would encourage rejection of the null hypothesis in favor of the alternative hypothesis that the mean of $X(0.5,\lambda)$ is in fact the largest of the three.

We now compute the distribution of $T_2(h,\lambda)$ under the null hypothesis. Without loss of generality, we may convert to standard units and take the common mean and standard deviation of the three random variables to be 0 and 1, respectively. Then the pdf of M is [30]

$$f_M(x) = 2f(x)F(x), \quad (19)$$

where ϕ and Φ are the pdf and cumulative distribution function (cdf) of a standard normal distribution. Therefore the pdf of T_2 is [30]

$$f_{T_2}(y) = \int_{-\infty}^{\infty} f(x+y) f_M(x)\,dx = \int_{-\infty}^{\infty} 2f(x)f(x+y)F(x)\,dx, \quad (20)$$

so that the complementary cdf is

$$P(T_2 \geq t) = \int_t^{\infty} \int_{-\infty}^{\infty} 2f(x)f(x+y)F(x)\,dx\,dy = \int_{-\infty}^{\infty} 2f(x)F(x)[1 - F(x+t)]\,dx. \quad (21)$$

Numerical computation of this integral gives the right-tail observed significance level.

In [33], we present the test statistics and observed significance levels for $T_2(0.02,\lambda)$ and $T_2(0.06,\lambda)$. For $\lambda \leq 0.84$, we have good statistical evidence that $\phi_c(0.5,\lambda)$ is larger than $\phi_c(0.5 \pm 0.06,\lambda)$. However, we cannot make this determination for $\lambda \geq 0.88$; this makes sense due to the flatness of these curves in Fig. 4.

We now turn to the case $h=0.02$. As seen in [33], we have good statistical evidence that $\phi_c(0.5,\lambda)$ is larger than $\phi_c(0.5 \pm 0.02,\lambda)$ for $\lambda \leq 0.2$. Unfortunately, for $\lambda \geq 0.25$, we do not have enough evidence to reject the null hypothesis that the means are the same. We note that, in this simulation for $\lambda=0.76$, our computation of $T_2(0.02,0.76)$ did yield a small observed significance level. However, since this did not occur for other comparable values of λ, we choose to retain the null hypothesis even for $\lambda=0.76$.

On the other hand, none of the test statistics $T_2(0.02,\lambda)$ are particularly negative, as evidenced by the fact that only one observed significance level is close to 1. A test statistic significantly less than zero would be evidence for the alternative hypothesis that either of $\phi_c(0.5 \pm h,\lambda)$ is larger than $\phi_c(0.5,\lambda)$. Therefore, for $\lambda \geq 0.25$, we also have no reason to think that $\phi_c(0.5,\lambda)$ is smaller than either $\phi_c(0.48,\lambda)$ or $\phi_c(0.52,\lambda)$.

We now summarize our findings in terms of $v^*(\lambda)$, the value at which $\phi_c(v,\lambda)$ is maximized. For $\lambda \leq 0.2$, we are confident that $0.48 < v^*(\lambda) < 0.52$. For $\lambda \leq 0.84$, we are confident that $0.44 < v^*(\lambda) < 0.56$. However, we do not have sufficient statistical evidence at this time for a more precise determination of $v^*(\lambda)$.

For the empirical fit given by Eq. (8), we find that

$$v^*(\lambda) = \frac{b(\lambda)}{b(\lambda) + c(\lambda)}. \quad (22)$$

These estimates of $v^*(\lambda)$ are presented in [33] and tend to be slightly less than 0.5. While both this direct empirical fit and the overall asymmetry of $\phi_c(v,\lambda)$ suggest that $\phi_c(v,\lambda)$ is not maximized at $v=0.5$, the statistical errors in the data do not allow us to conclusively say that $v^*(\lambda) \neq 0.5$. Perhaps, with more refined studies, it can be shown conclusively that the peak is not at $v=0.5$.

IV. CONCLUSIONS

We have used the frontier-walk method of continuum gradient percolation to measure the percolation threshold (or critical volume fraction) $\phi_c(v,\lambda)$ as a function of λ, the ratio of the smaller and larger disk radii, and v, the volumetric proportion of the smaller disks. We have shown that the conjectured symmetry of $\phi_c(v,\lambda)$ as a function of v does not hold; while the function is nearly symmetric, the asymmetry is quite unmistakable, as seen quite clearly in Fig. 5. We have pinpointed where the argument for symmetry in [26] is incomplete. We have also separately studied the statistics on the location of the peak of the curve, but cannot say unambiguously that it is not at $v=1/2$.

While $\phi_c(v,\lambda)$ is not exactly symmetric, its near symmetry is notable, and there is at present no theoretical reason for this behavior. A systematic theory that would predict the behavior of $\phi_c(v,\lambda)$, as opposed to an empirical fit such as Eq. (8), would be a welcome addition to the percolation literature.

ACKNOWLEDGMENTS

The computational support provided by Academic Computing and User Services at the University of North Texas is acknowledged. This work was supported in part by National Science Foundation Grant No. DMS-0553487 (R.M.Z.).

[1] D. Stoyan, W. S. Kendall, and J. Mecke, *Stochastic Geometry and Its Applications*, 2nd edition (Wiley, New York, 1995).
[2] K. R. Mecke, in *Statistical Physics and Spatial Statistics*, edited by K. R. Mecke and D. Stoyan (Springer, New York, 2000).
[3] J. Quintanilla and S. Torquato, J. Chem. Phys. **111**, 5947 (1999).
[4] J. Quintanilla, S. Torquato, and R. M. Ziff, J. Phys. A **33**, L399 (2000).
[5] M. K. Phani and D. Dhar, J. Phys. A **17**, L645 (1984).
[6] B. Lorenz, I. Orgzall, and H.-O. Heuer, J. Phys. A **26**, 4711 (1993).
[7] J. Quintanilla, Phys. Rev. E **63**, 061108 (2001).
[8] J. Quintanilla, Mech. Mater. **38**, 849 (2006).
[9] D. R. Baker, G. Paul, S. Sreenivasan, and H. E. Stanley, Phys. Rev. E **66**, 046136 (2002).
[10] K. R. Mecke and A. Seyfried, Europhys. Lett. **58**, 28 (2002).
[11] Y.-B. Yi and A. M. Sastry, Phys. Rev. E **66**, 066130 (2002).
[12] Y.-B. Yi, C.-W. Wang, and A. M. Sastry, J. Electrochem. Soc. **151**, A1292 (2004).
[13] C. D. Lorenz and R. M. Ziff, J. Chem. Phys. **114**, 3659 (2001).
[14] R. Consiglio, D. R. Baker, G. Paul, and H. E. Stanley, Physica A **319**, 49 (2003).
[15] J. Kertész, J. Phys. (France) Lett. **41**, L393 (1981).
[16] W. T. Elam, A. R. Kerstein, and J. J. Rehr, Phys. Rev. Lett. **52**, 1516 (1984).
[17] M. D. Rintoul, Phys. Rev. E **62**, 68 (2000).
[18] Y. B. Yi, Phys. Rev. E **74**, 031112 (2006).
[19] P. Hall, Ann. Probab. **13**, 1250 (1985).
[20] P. Hall, *Introduction to the Theory of Coverage Processes* (Wiley, New York, 1988).
[21] R. Meester, R. Roy, and A. Sarkar, J. Stat. Phys. **75**, 123 (1994).
[22] R. Meester and R. Roy, *Continuum Percolation* (Cambridge University Press, London, 1996).
[23] J. Jonasson, Ann. Probab. **29**, 624 (2001).
[24] R. Roy and H. Tanemura, Adv. Appl. Probab. **34**, 48 (2002).
[25] P. Balister, B. Bollobás, and M. Walters, Random Struct. Algorithms **26**, 392 (2005).
[26] R. Consiglio, R. N. A. Zouain, D. R. Baker, G. Paul, and H. E. Stanley, Physica A **343**, 343 (2004).
[27] D. Stauffer and A. Aharony, *Introduction to Percolation Theory* (Taylor and Francis, London, 1994).
[28] S. Zuyev and J. Quintanilla, J. Math. Phys. **44**, 6040 (2003).
[29] R. M. Ziff and B. Sapoval, J. Phys. A **19**, L1169 (1986).
[30] J. Pitman, *Probability* (Springer, New York, 1993).
[31] S. Torquato, *Random Heterogeneous Materials: Microstructure and Macroscopic Properties* (Springer-Verlag, New York, 2002).
[32] J. A. Rice, *Mathematical Statistics and Data Analysis*, 2nd edition (Duxbury, Belmont, CA, 1994).
[33] See EPAPS Document No. E-PLEEE8-76-156710 for our measurements of $\phi_c(v,\lambda)$, the fit to Eq. (9), and the observed significance levels of the test statistics $T_1(\lambda)$ and $T_2(h,\lambda)$. For more information on EPAPS, see http://www.aip.org/pubservs/epaps.html.
[34] B. Sapoval, M. Rosso, and J. F. Gouyet, J. Phys. (France) Lett. **46**, L149 (1985).